

1 *Type of the Paper (Article)*

## 2 **Liquid-Phase Epitaxial Growth and Characterization** 3 **of Nd:YAl<sub>3</sub>(BO<sub>3</sub>)<sub>4</sub> Optical Waveguides**

4 **Yi Lu, Peter Dekker and Judith M Dawes \***

5 MQ Photonics, Department of Physics and Astronomy, Macquarie University, Sydney

6 \* Correspondence: Judith.dawes@mq.edu.au ; Tel.: + 61 – 2 98508903

7

8 **Abstract:** We investigated fabrication of neodymium doped thin film optical waveguide-based  
9 devices as potential active sources for planar integrated optics. Liquid-phase epitaxial growth was  
10 used to fabricate neodymium-doped yttrium aluminum borate films on compatible lattice-matched  
11 un-doped yttrium aluminum borate substrates. We observed the refractive index contrast of the  
12 doped and un-doped crystal layers by differential interference contrast microscopy. In addition,  
13 characterization by X-ray powder diffraction, optical absorption and luminescence spectra  
14 demonstrated the crystal quality and uniformity and optical guiding of the resulting thin films.

15 **Keywords:** thin film crystal growth; epitaxial layer growth; multifunctional borate crystals;  
16 planar optical waveguides

17

---

### 18 **1. Introduction**

19 Integrated optics and photonics is increasingly important for optical signal processing in many  
20 applications, and relies on the development of compact, robust planar optical devices. Integrated  
21 optics employs waveguides as the building blocks for optical components which are then connected  
22 into circuits [1]. In particular, integrated optical systems using waveguide-based components  
23 typically include active devices such as lasers and modulators integrated into photonic circuits, and  
24 in each case, the structure must be designed to guide and confine the light within the active region of  
25 the device by careful design of the refractive index contrast between the cladding and the active layer.  
26 Optical waveguides are described as single mode or multimode based on the properties of the  
27 structure, as determined by the refractive index and dimensions of the guiding layer and substrate  
28 or cladding [2]. Active waveguide devices offer particular advantages over their bulk counterparts  
29 because the optical confinement increases the intensity of the signal and pump light within the  
30 waveguide, hence ensuring that the amplification or nonlinear optical frequency conversion can be  
31 more efficient than in comparable bulk devices [3]. Here we consider multimode active planar  
32 dielectric devices.

33 Fabrication of planar waveguide devices has been accomplished by a variety of approaches [3].  
34 For example, the refractive index inside a dielectric material may be modified using nonlinear  
35 multiphoton processes [4, 5], or ion-exchange [6]. In another approach, two crystals may be optically  
36 polished and then thermally bonded to achieve strong adhesion between the crystal layers [7]. This  
37 typically requires careful polishing to ensure that the active layer is sufficiently thin. Epitaxial growth  
38 processes [8] such as liquid phase epitaxy (LPE) [9], pulsed laser deposition [10], molecular beam  
39 epitaxy (MBE) [11], hydrothermal epitaxy [12], metal oxide chemical vapor deposition (MOCVD)  
40 [13], or halide vapor phase epitaxy (HVPE) [14], enable production of high quality crystalline  
41 materials, which are practical for waveguide fabrication.

42 There has been long-standing interest in multifunctional doped borate laser crystals [10-19], for  
43 use in compact robust lasers emitting fundamental or self-frequency-doubled wavelengths, with Q-  
44 switched, mode-locked or continuous wave operation. The thermal conductivity of these crystals

45 facilitates the operation of the lasers at high power and in thin disk geometries [20-22], and un-doped  
46 borates have been adopted for nonlinear optics [23, 24]. This has led to a new drive for improved  
47 growth techniques for these crystals. Various approaches to optimize the crystal growth; the choice,  
48 preparation, and mixing of the flux, and the temperature profile, have been reported [10-12]. There  
49 is a balance between the relatively slow growth of the crystals, and the control of the crystal phase  
50 and uniformity, due to the formation of crystal twins [25, 26]. However, following an early report of  
51 epitaxial film growth [27], there has been recent interest to develop borate crystals for waveguide  
52 devices compatible with integrated optics, because this geometry enables concentration of the light  
53 in the active layer to enhance both the amplification and the optical nonlinearity of the device [28-  
54 31].

55 The liquid phase epitaxial growth technique has several advantages compared with other  
56 waveguide fabrication techniques. The layers are grown isothermally with homogeneous  
57 composition, so the quality of the epitaxial layer is comparable with that of bulk materials. The  
58 interface between the thin film and the substrate exhibits a step profile in the refractive index whereas  
59 other waveguide fabrication techniques typically lead to graded index profiles. Generally, the modes  
60 propagating inside a multimode step index profile structure have uniform effective index, whereas  
61 for a graded index profile, different modes have different effective index. The thickness of the  
62 waveguide structure can be controlled accurately by the growth duration and growth temperature.  
63 Finally, liquid phase epitaxy is adaptable for any single crystalline layer or active dopant, using an  
64 appropriate flux system and growth conditions [8].

65 We investigated liquid phase epitaxy as an effective growth method for Nd:YAl<sub>3</sub>(BO<sub>3</sub>)<sub>4</sub>  
66 (Nd:YAB) thin films on compatible lattice-matched un-doped borate substrates. The resulting films,  
67 whose lattice constants are consistent with R32 crystal symmetry, exhibit very good optical  
68 properties. Differential interference contrast microscopy, X-ray powder diffraction and optical  
69 absorption and luminescence spectra were used to characterize the optical quality and uniformity of  
70 these thin films.

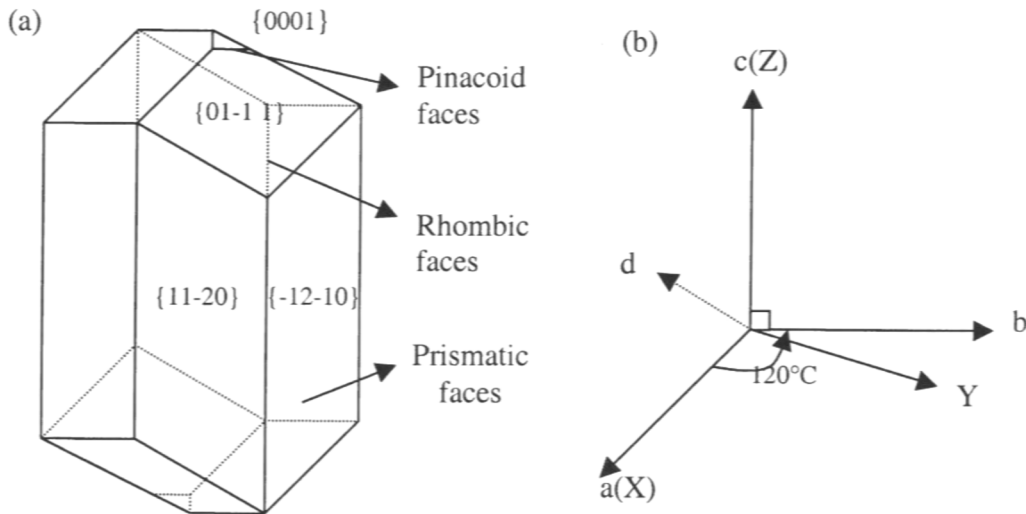
## 71 2. Crystal Growth

### 72 2.1. Crystal growth methods

73 The flux system for the Nd:YAB epitaxial growth was chosen to be K<sub>2</sub>Mo<sub>3</sub>O<sub>10</sub> with excess Y<sub>2</sub>O<sub>3</sub>  
74 and B<sub>2</sub>O<sub>3</sub> [11]. This flux system offers advantages because it has lower volatility than the PbF<sub>2</sub>-3B<sub>2</sub>O<sub>3</sub>  
75 flux system, and excess Y<sub>2</sub>O<sub>3</sub> and B<sub>2</sub>O<sub>3</sub> were added to the initial flux to suppress Al<sub>5</sub>BO<sub>9</sub> inclusions  
76 and to compensate for the volatility of B<sub>2</sub>O<sub>3</sub> during crystal growth [11]. The mix for the growth was  
77 calculated as 8 at.% Nd/(Nd + Y) with 24.4 wt% of Nd:YAB in the solution. The solvent composition  
78 was 91.9wt% of K<sub>2</sub>Mo<sub>3</sub>O<sub>10</sub> + 5.4wt% B<sub>2</sub>O<sub>3</sub> + 0.25 wt% Y<sub>2</sub>O<sub>3</sub>. All the chemicals were obtained from  
79 local suppliers, and heat treated in a 300 C furnace to remove adsorbed water before weighing. They  
80 were completely ground and mixed in the platinum crucible (5 cm diameter) and heated in an electric  
81 resistance furnace at 1150 °C for 24 hours. The temperature was then dropped to about 1000 C to  
82 find the actual saturation point by repeated seeding. The seed was settled to the mid part of the  
83 solution to ensure a homogeneous temperature gradient.

84 The substrate for the thin film growth needs to be selected carefully – it must permit reasonable  
85 lattice matching with the epitaxial layer to avoid strain due to lattice mismatch, and it must ensure a  
86 refractive index contrast, so that the active layer is the guiding layer with a higher refractive index.  
87 We selected un-doped YAl<sub>3</sub>(BO<sub>3</sub>)<sub>4</sub> (YAB) as it satisfies these criteria well. We also determined that a  
88 neodymium fraction of 8% permitted waveguide confinement, without excessive lattice mismatch.  
89 The calculated refractive index contrast for 8 at.% Nd dopant are 0.0632 for n<sub>o</sub> and 0.0608 for n<sub>e</sub> [11].

90 Figure 1 (a) shows the prismatic faces  $\{11\bar{2}0\}$  and  $\{2\bar{1}\bar{1}0\}$  and the rhombic face  $\{01\bar{1}1\}$  for Nd:YAB, along  
91 with the crystal axes in Figure 1 (b). Previous liquid phase epitaxial growth of NdAB yielded thin  
92 films of good quality using  $\text{Gd}_{0.59}\text{La}_{0.41}\text{Al}_3(\text{BO}_3)_4$  substrates with growth rates of around 1  $\mu\text{m}/\text{min}$  [32].  
93  
94



95

96

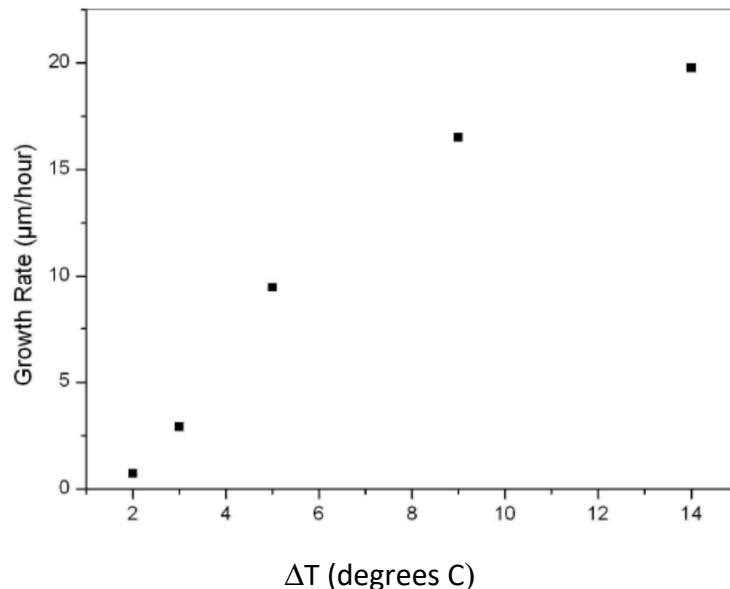
Figure 1(a) The growth habit of Nd:YAB crystals; (b) The hexagonal crystal axes for the crystals

97

98 The substrates were cut on the rhombic face  $\{01\bar{1}1\}$  from bulk YAB crystals grown in our own  
99 laboratory and that of Prof. N. Leonyuk. The surfaces of the substrates were left unpolished. The  
100 substrates were dipped vertically into the melt with platinum wire wrapping the top of the substrates.  
101 The  $\{01\bar{1}1\}$  cut pure YAB substrate (typical dimension 1 mm X 2 mm X 5 mm) was introduced and  
102 placed in the center of the flux in the crucible.

103 Liquid phase epitaxial growth of thin films is typically similar to that of bulk crystals. However  
104 the temperature is selected to be below the saturation point to allow thermodynamic growth of layers  
105 with the same orientation as the substrate while immersed in a super-saturated solution. At  
106 conditions which are close to equilibrium, the deposition of the crystal on the substrate is slow and  
107 uniform. In our case, the temperature was initially set to 1 °C above the saturation point to smooth  
108 and dissolve the surface (which becomes the substrate – film interface) and the temperature was then  
109 ramped down to 4 °C below the saturation point (around 1000 °C) to start thin film growth. The  
110 growth rate was about 5  $\mu\text{m}$  per hour at this temperature, (see Figure 2). This growth condition was  
111 chosen to ensure the thermodynamic growth regime and avoid any risk of spontaneous nucleation  
112 (which appears to occur for  $\Delta T$  of 8 °C or more). After growth, the substrate was carefully removed  
113 from the flux and slowly cooled down to room temperature over 24 hours. Bulk Nd:YAB crystals  
114 were also grown in our lab using the liquid phase epitaxy technique in the same solution. The solution  
115 mix was as for thin film growth, with a small YAB seed.  
116

117



118

119  
120

Figure 2: Nd:YAB crystal growth rate on rhombic face  $\{01\bar{1}1\}$  seed crystal vs temperature below saturation.

121

### 2.2. Results of Crystal Growth

122  
123  
124  
125  
126  
127  
128  
129  
130  
131  
132  
133  
134

Figure 3a) shows an image of an as-grown Nd:YAB bulk crystal, with the growth facets visible, grown for two weeks under similar conditions as for the thin films, with the temperature ramping down by 0.5 C per day.. Figure 3b) shows an as-grown Nd:YAB crystalline thin film with un-doped YAB substrate that has been side-polished and imaged by differential interference contrast microscope (Olympus BX60). The Nd:YAB thin film layer appears as a uniform, smooth blue stripe in the microscope image with a sharp change and an apparent phase contrast with the pure YAB substrate, which suggests a step-like refractive index profile. The film thickness was measured to be  $71 \pm 0.5 \mu\text{m}$ . The film shown in Figure 3b) was obtained after epitaxial growth for 12 hours at the conditions specified above. The as-grown thin film sample was transparent and homogeneous with a smooth surface. No noticeable crystallites of the monoclinic form of Nd:YAB were obtained, as discussed in Ref [30]; we attribute this to the moderate Nd dopant fraction and lower temperature growth process that we used.



135

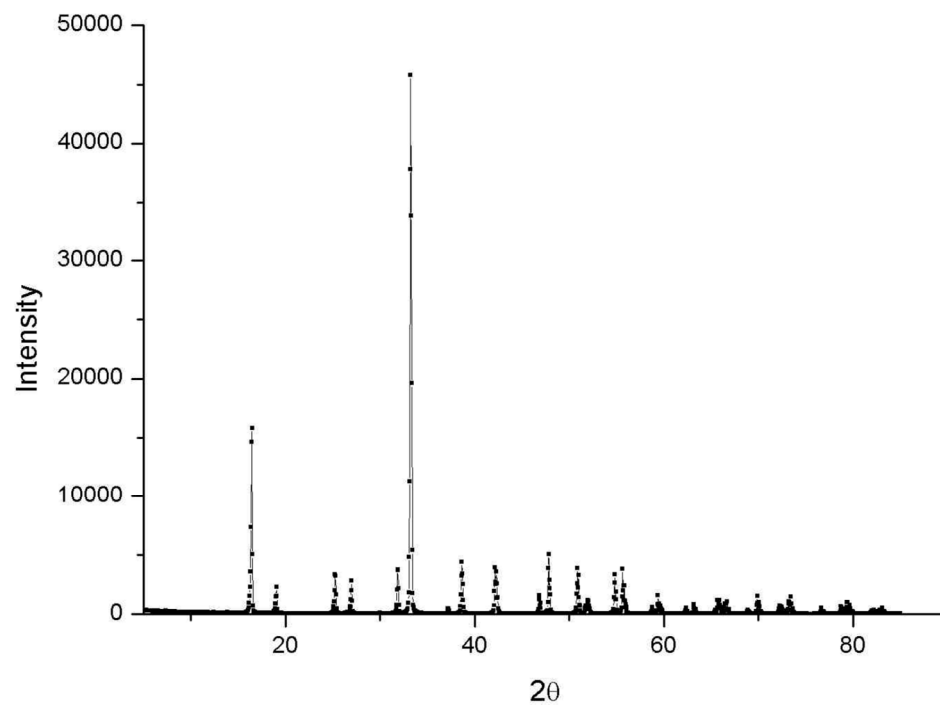
136  
137

Figure 3a). As-grown bulk Nd:YAB crystal, and Figure 3b) Differential interference contrast image of the Nd:YAB thin film and YAB substrate in cross-section.

## 138 3. Crystal Characterization Methods and Results

## 139 3.2. Crystal Characterization Results

140 X-ray powder diffraction was used to characterize the crystallographic structure and the results  
141 were compared with the diffraction patterns in an existing database. The X-ray powder diffraction  
142 (XRD) pattern of ground Nd:YAB bulk crystals grown by top-seeded solution growth was measured  
143 using a D/max-rA type X-ray diffractometer and CuK $\alpha$  radiation ( $\lambda = 1.54056 \text{ \AA}$ ) at room temperature,  
144 and is shown in Figure 4. The X-ray powder diffraction pattern of the Nd:YAB crystals was found to  
145 be consistent with the reference pattern of YAl<sub>3</sub>(BO<sub>3</sub>)<sub>4</sub> (JCPDS card No. 15-117) [32], indicating that  
146 the neodymium dopant does not significantly perturb the lattice and the crystal belongs to the R32  
147 space group. The lattice parameters were calculated by the least-squares method.



148  
149 Figure 4: X-ray powder diffraction for as-grown Nd:YAB crystal  
150

151 According to the X-ray diffraction data, the calculated lattice constants of the Nd:YAB crystals  
152 were  $a = b = 9.298 \text{ \AA}$ ,  $c = 7.2406 \text{ \AA}$ . In comparison with the data presented in Ref [11], the measured  
153 lattice constants of the bulk Nd:YAB crystal were close to those of Nd<sub>0.09</sub>Y<sub>0.91</sub>Al<sub>3</sub>(BO<sub>3</sub>)<sub>4</sub>, which were  
154 9.295  $\text{\AA}$  and 7.236  $\text{\AA}$ , which is consistent with 9 at.% N dopant concentration. Lattice constants of YAB  
155 crystals with different dopants are listed in Table 1. Assuming that the thin film has similar Nd  
156 concentration to that of the bulk crystal, the lattice mismatch of the as-grown Nd:YAB thin film is  
157 about 0.11% and 0.2% for the lattice constants  $a$  and  $c$  respectively. From optical microscopy and  
158 visual inspection the Nd dopant distribution in the film appeared uniform. This is expected as the  
159 solute concentration does not vary significantly during thin film growth.

160  
161  
162

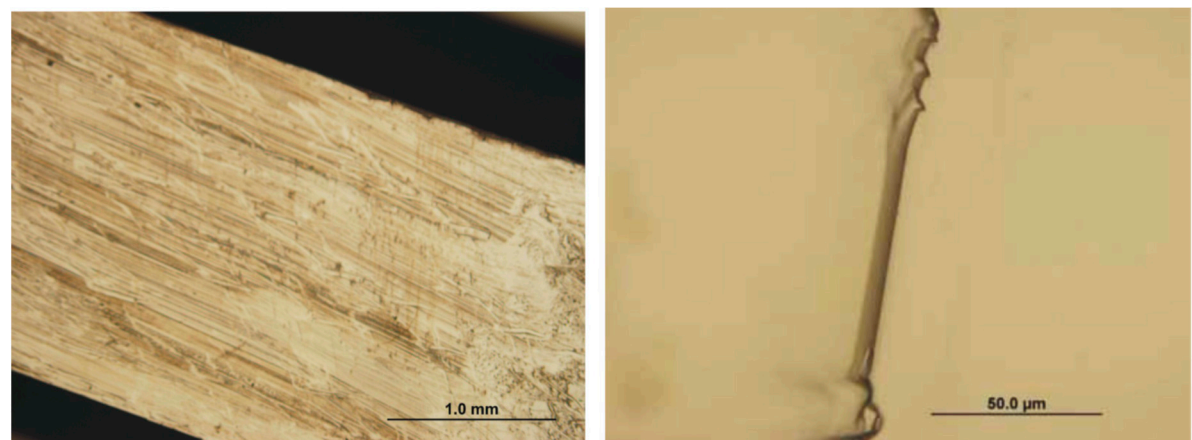
163

**Table 1.** Lattice parameters of  $\text{YAl}_3(\text{BO}_3)_4$ 

Crystals	$a$ (Å)	$c$ (Å)	Reference
YAB (JCPDS No. 15-117)	9.2872	7.2433	[32]
$\text{Nd}_{0.09}\text{Y}_{0.91}\text{Al}_3(\text{BO}_3)_4$	9.295	7.236	[11]
$\text{NdAl}_3(\text{BO}_3)_4$	9.365	7.262	[11]
Nd:YAB crystal	9.298	7.2406	This work

164

165



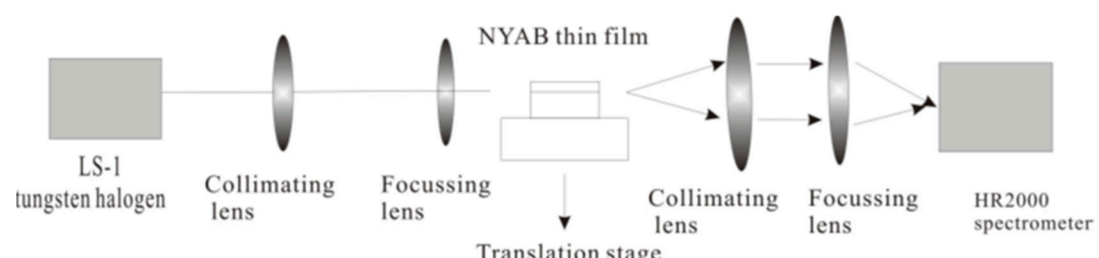
166

167 Figure 5 (a): Microscope images of substrate surface (5  $\times$ ) and (b) after growth thin film surface (20  $\times$ ) for  
 168 Nd:YAB on a YAB substrate. The substrate is held vertically in the flux

169

170 The substrate crystal surface quality is shown in Figure 5a) before thin film growth, and it shows  
 171 the rough unpolished surface, which was smoothed in the initial period of higher melt temperature.  
 172 Figure 5b) shows the as-grown crystalline film image in cross-section. The epitaxial growth results in  
 173 a smooth surface with no additional crystallite formation. For the purposes of crystal  
 174 characterization, the absorption spectrum of a 2 mm  $\times$  4 mm  $\times$  1.1 mm slice cut and polished from a  
 175 bulk Nd:YAB crystal was measured using a Cary 5E spectrophotometer. This was compared with the  
 176 absorption along the guiding direction of the epitaxial layer as measured in the set up shown in  
 177 Figure 6. Figure 7a) shows the (unpolarized) absorption spectrum of bulk Nd:YAB (thickness 1.1 mm)  
 178 in the wavelength range 300 - 1000 nm. There are six main absorption peaks in the spectrum at 360,  
 179 528, 588, 750, 809, and 882 nm, which may be assigned according to Ref [11]. The uncorrected  
 180 absorption spectrum for the thin film is illustrated in Figure 7b). The absorption peak positions and  
 181 features are similar to those for the bulk sample. The drifting base line is attributed to the wavelength  
 182 response of the detector in the Ocean Optics HR2000 spectrometer.

183



184

185

Figure 6: Experimental setup for measuring absorption spectra along guiding direction

186

187

188

189

190

191

192

193

194

195

196

197

198

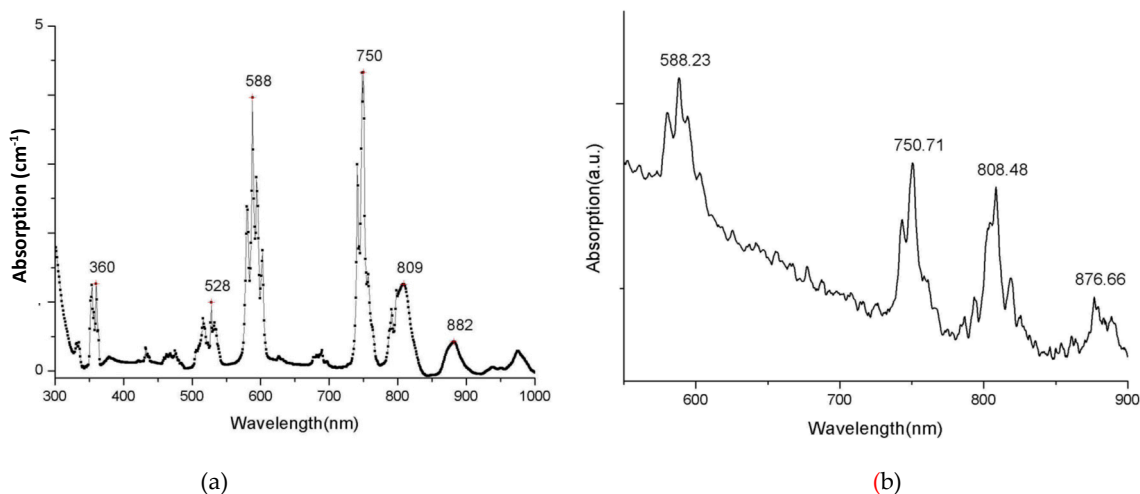
199

200

201

202

203



(a)

(b)

Figure 7 (a) Absorption spectrum of a polished slice of bulk Nd:YAB and (b) Uncorrected absorption spectrum of Nd:YAB crystalline thin film, along the guiding direction, showing intensity peaks at 588, 750 and 808 nm, attributed to transitions from  $^4I_{9/2}$  to  $^4G_{5/2}$ ,  $^4F_{7/2}$  and  $^2H_{9/2}$  respectively.

204

The near-infrared fluorescence spectra of the Nd:YAB thin film (thickness 71  $\mu$ m), and a bulk Nd:YAB crystal sample at room temperature are overlaid in Figure 7. This spectrum was obtained by coupling light from an 808 nm diode laser into the thin film and focussing the output by a lens into a fibre-coupled spectrometer. The 887 nm, 1062 nm and 1339 nm peaks correspond to the fluorescence of the  $^4F_{3/2}$  level into the  $^4I_{9/2}$ ,  $^4I_{11/2}$ , and  $^4I_{13/2}$  multiplets, respectively. The room temperature fluorescence peak at 1062 nm is very strong, and the bandwidth (FWHM) of the 1062 nm peak is about 10 nm. The fluorescence spectrum of the thin film Nd:YAB crystal is well-correlated with that of the bulk Nd:YAB sample.

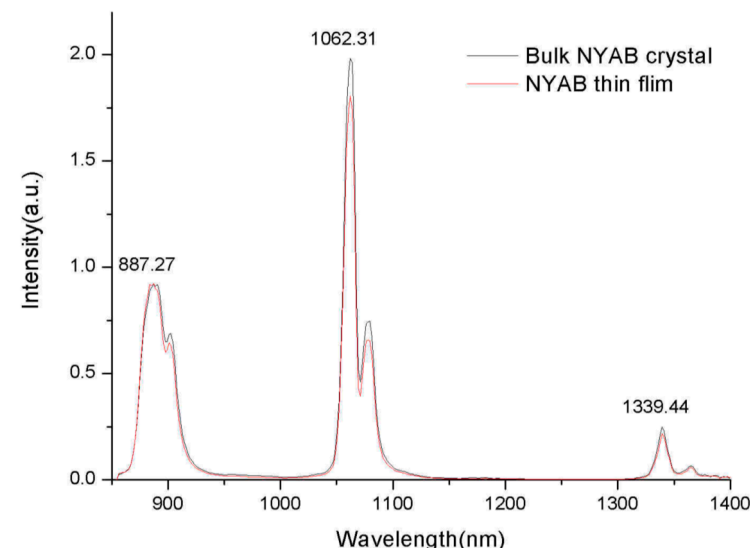


Figure 8: Luminescence spectrum of Nd:YAB thin film overlaid with that of the bulk Nd:YAB sample

212

213

214

215

216

217

218

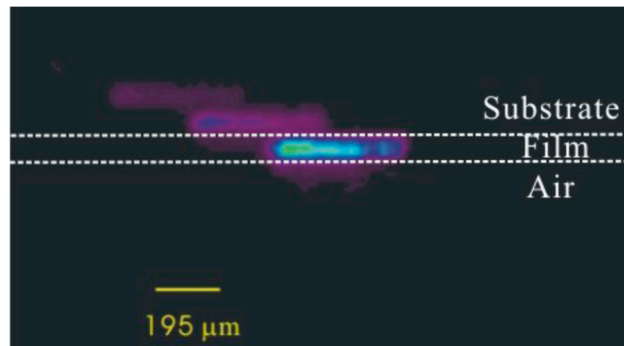
219

220

221

A near-field image of the Nd:YAB thin film luminescence emitted from the end of the waveguide, as longitudinally pumped by the 808 nm diode laser, is shown in Figure 9. This was captured by a CCD camera (Pulnix) through a 1064 nm band pass filter. The camera was coupled to a laser beam analyser (Spiricon LBA100A). The luminescence image size is about 71  $\mu$ m in the guided direction and 400  $\mu$ m in the unguided direction. Two subsidiary images, probably due to back reflections, are also observable to the upper left. This image shows strong evidence of effective guiding within the epitaxial film layer.

222



223

224

225

Figure 9 Luminescence image of Nd:YAB thin film, (image artefacts to the upper left).

#### 226 4. Discussion and Conclusions

227 Nd:YAB planar waveguides with 9% Nd dopant were successfully grown by the top-seeded  
228 solution method from the  $K_2Mo_3O_{10}$  and  $B_2O_3$  flux system. The growth rates were measured and the  
229 growth conditions and procedure were selected for high quality film growth in the thermodynamic  
230 regime. Nd:YAB thin film layers were obtained at 4 °C below the saturation temperature with a  
231 growth rate about 5  $\mu\text{m}/\text{hour}$  on an un-doped {0111} YAB substrate. The growth of the thin films  
232 occurred over about 12 hours, with additional time for cooling. The as-grown thin films have good  
233 surface and optical quality and homogeneity, and exhibit effective waveguiding of the strong  
234 luminescence at 1062 nm. Future measurements of the optical gain and transmission losses in the  
235 devices are planned.

236 **Author Contributions:** Conceptualization JMD and YL; crystal growth methods and experiments YL;  
237 crystal characterization YL and PD; writing JMD and YL with editing by PD; project administration  
238 JMD.

239 **Funding:** The authors acknowledge funding support to establish the crystal growth and  
240 characterization facility by Macquarie University and the Australian Research Council.

241 **Acknowledgments:** The authors acknowledge valuable advice and discussions on crystal growth  
242 and flux preparation from Prof Nikolay Leonyuk and Prof Robert Feigelson. Prof Leonyuk provided  
243 bulk YAB crystals which were used as substrates for the thin film growth.

244 **Conflicts of Interest:** The authors declare no conflict of interest. The funders had no role in the design  
245 or the study, collection and analysis of data, manuscript writing, or publication decision.

#### 246 References

1. Tien, P.K.; Light waves in thin films and integrated optics. *Appl Opt* **1971**, *10*, 2395-2413.
2. Snyder, A.W.; Love, J.; *Optical Waveguide Theory*. Chapman and Hall, London U.K., 1983, pp 6-26, ISBN 0 412 24250 8
3. Mackenzie, J.I.; Dielectric solid state planar waveguide lasers: a review. *IEEE J Sel Top Quantum Electron* **2007**, *13*, 626-637.
4. Chen, F.; Vazquez de Aldana, J.R.; Optical waveguides in crystalline dielectric materials produced by femtosecond-laser micromachining. *Laser Photonics Rev.* **2014**, *8*, 251-275, DOI 10.1002/lpor.201300025
5. Ams, M.; Marshall, G.D.; Dekker, P.; Piper, J.A.; Withford, M.J. Ultrafast laser-written active devices, *Laser Photon Reviews* **2009**, *3*, 535-544 doi.org/10.1002/lpor.200810050
6. Honkanen, S.; West, B.R.; Tliniemi, S.; Madasamy, P.; Morrell, M.; Auxier, J.; Geraghty, D.; Recent advances in ion exchanged glass waveguides and devices. *Phys Chem. Glasses Eur J. Glass Sci. Technol. B.* **2006**, *47*, 110-120

259 7. Brown, C.T.A.; Bonner, C.L.; Warburton, T.J.; Shepherd, D.P.; Tropper, A.C.; Hanna, D.C.; Meissner, H.E.  
260 Thermally bonded planar waveguide lasers, *Appl. Phys. Lett.*, **1997**, *71*, 1139–1141.

261 8. Capper P., Irvine S., Joyce T. (2017) Epitaxial Crystal Growth: Methods and Materials. In: Kasap S.,  
262 Capper P. (eds) Springer Handbook of Electronic and Photonic Materials. Springer Handbooks.  
263 Springer, Cham

264 9. Ferrand, B.; Chambaz, B.; Couchaud, M.; Liquid phase epitaxy: A versatile technique for the development  
265 of miniature optical components in single crystal dielectric media, *Opt. Mat.* **1999**, *11* 101-114  
266 doi.org/10.1016/S0925-3467(98)00037-8

267 10. Beecher, S.J.; Grant-Jacob, J.A.; Hua, P.; Prentice, J.J.; Eason, R.W.; Shepherd, D.P.; Mackenzie, J.I.  
268 Ytterbium-doped-garnet crystal waveguide lasers grown by pulsed laser deposition. *Opt. Mater.*  
269 *Express* **2017**, *7*, 1628-1633 doi.org/10.1364/OME.7.001628

270 11. Cho, A.Y.; Advances in Molecular Beam Epitaxy. *J. Cryst. Growth.* **1991**, *111*, 1-13. doi.org/10.1016/0022-  
271 0248(91)90938-2

272 12. Terry, R.J.; McMillen, C.D.; Chen, X.; Wen, Y.; Zhu, L.; Chumanov, G.; Kolis, J.W.; Hydrothermal single  
273 crystal growth and second harmonic generation of Li<sub>2</sub>SiO<sub>3</sub>, Li<sub>2</sub>GeO<sub>3</sub>, and Li<sub>2</sub>Si<sub>2</sub>O<sub>5</sub>. *J. Cryst Growth*, **2018**,  
274 *493*, 58-64 doi.org/10.1016/j.jcrysgro.2018.02.028

275 13. Sun, H.; Li, K.H.; Torres Castanedo, C.G.; Okur, S.; Tompa, G.S.; Salagaj, T.; Lopatin, S.; Genovese, A.; Li,  
276 X.; HCl Flow-Induced Phase Change of  $\alpha$ -,  $\beta$ -, and  $\varepsilon$ -Ga<sub>2</sub>O<sub>3</sub> Films Grown by MOCVD, *Cryst Growth*  
277 *Design* **2018** *18*, 2370-2376 DOI: 10.1021/acs.cgd.7b01791

278 14. Tashev, V.; Vangala, S.; Peterson, R.; Kimani M.; Snure, M.; Markov, I.; Homo and heteroepitaxial growth  
279 and study of orientation-patterned GaP for nonlinear frequency conversion devices. Proc. SPIE 9731,  
280 Nonlinear Frequency Generation and Conversion: Materials, Devices, and Applications XV, 97310G (4  
281 March 2016); Vodopyanov, K.L.; Schepler, K.L.; Eds doi: [10.1117/12.2217464](https://doi.org/10.1117/12.2217464)

282 15. Ballman, A.A.; A new series of synthetic borates isostructural with the carbonate mineral huntite. *Am*  
283 *mineral*, **1962**, *47*, 1380-1383.

284 16. Leonyuk, N.I.; Leonyuk, L.I.; Growth and characterization of RM<sub>3</sub>(BO<sub>3</sub>)<sub>4</sub> crystals. *Prog. Cryst. Growth*  
285 *Charact.* **1995**, *31*, 179-278 doi.org/10.1016/0960-8974(96)83730-2

286 17. Wang, P.; Dawes, J.M.; Dekker, P.; Knowles, D.S.; Piper, J.A.; Lu, B.S. Growth and evaluation of ytterbium  
287 doped yttrium aluminum borate as a potential self-doubling laser crystal. *J. Opt. Soc. Am B*, **1999**, *16*, 63-69  
288 doi.org/10.1364/JOSAB.16.000063

289 18. Jaque, D.; Enguita, O.; Garcia Sole, J.; Jiang, A.D.; Luo, Z.D.; Infrared continuous wave laser gain in  
290 neodymium aluminum borate: a promising candidate for microchip diode-pumped solid-state lasers. *Appl*  
291 *Phys. Lett.* **2000**, *76*, 2176-2178. doi.org/10.1063/1.126289

292 19. Wang, P.; Dekker, P.; Dawes, J.M.; Piper, J.A.; Liu, Y.G.; Wang, J.Y.; Efficient continuous wave self-  
293 frequency doubling green diode pumped Yb:YAB lasers. *Opt. Lett.* **2000**, *25*, 731-733  
294 doi.org/10.1364/OL.25.000731

295 20. Dekker, P.; Dawes, J.M.; Piper, J.A.; Liu, Y.G. Wang, J.Y.; 1.1W CW self-frequency doubled diode-pumped  
296 Yb:YAl<sub>3</sub>(BO<sub>3</sub>)<sub>4</sub> laser. *Opt. Commun.* **2001**, *195*, 431-436 doi.org/10.1364/ASSL.2001.WA3

297 21. Lederer, M.J.; Hildebrandt, M.; Kolev, V.Z.; LutherDavies, B.; Taylor, B.; Dawes, J.M.; Dekker, P.; Piper,  
298 J.A.; Tan, H.H.; Jagadish, C.; Passive mode locking of a self-frequency doubling Yb:YAl<sub>3</sub>(BO<sub>3</sub>)<sub>4</sub> laser, *Opt*  
299 *Lett.* **2002**, *27*, 436-438 doi.org/10.1364/OL.27.000436

300 22. Dekker, P.; Dawes, J.M.; Piper, J.A.; 2.27 W Q-switched self-doubling Yb:YAB laser with controllable pulse  
301 length. *J. Opt. Soc. Am B*, **2005**, *22*, 378-384 doi.org/10.1364/JOSAB.22.000378

302 23. Chen, Y.J.; Lin, Y.F.; Gong, X.H.; Tan, Q.G.; Luo, Z.D.; Huang, Y.D.; 2.0 W diode-pumped Er,Yb:YAl<sub>3</sub>(BO<sub>3</sub>)<sub>4</sub>  
303 efficient 1.5  $\mu$ m laser crystal. *Appl Phys. Lett.* **2006**, *89*, 241111. doi.org/10.1063/1.2404969

304 24. Lagatsky, A.A.; Sibbett, W.; Kisel, V.E.; Troshin, A.E.; Tolstik, N.A.; Kuleshov, N.V.; Leonyuk, N.L.;  
305 Zhukov, A.E.; Rafailov, E.U.; Diode-pumped passively mode locked Er,Yb:YAl<sub>3</sub>(BO<sub>3</sub>)<sub>4</sub> laser at 1.5-1.6  $\mu$ m.  
306 *Opt Lett.* **2008**, *33*, 83-85 doi.org/10.1364/OL.33.000083

307 25. Blows, J.L.; Dekker, P.; Wang, P.; Dawes, J.M.; Omatsu, T.; Thermal lensing measurements and thermal  
308 conductivity of Yb:YAB. *Appl. Phys. B*, **2003**, *76*, 289-292 doi.org/10.1007/s00340-002-1092-4

309 26. Liu, J.; Mateos, X.; Zhang, H.J.; Li, J.; Wang, J.Y.; Petrov, V.; High power laser performance of Yb:YAl<sub>3</sub>(BO<sub>3</sub>)<sub>4</sub>  
310 crystals cut along the crystallographic axes. *IEEE J Quantum Electron.* **2007**, *43*, 385-390  
311 DOI: 10.1109/JQE.2007.893900

312 27. Weichert, B.; Rumpf, M.; Voss, A.; Wesemann, V.; Rytz, D.; Abdou Ahmed, M.; Graf, T.; Yb:YAl<sub>3</sub>(BO<sub>3</sub>)<sub>4</sub> as  
313 gain material in thin disk oscillators: demonstration of 109 W of IR output power. *Opt Expr.* **2013**, *21*, 25709,  
314 doi:10.1364/OE.21.025708

315 28. Yu, X.; Yue, Y.; Yao, J.; Hu, Z.G.; YAl<sub>3</sub>(BO<sub>3</sub>)<sub>4</sub> crystal growth and characterization. *J. Cryst. Growth.* **2010**, *312*,  
316 3029-3033 doi.org/10.1016/j.jcrysGro.2010.07.005

317 29. Yu, J.; Liu, L.; Zhai, N.; Zhang, X.; Wang, G.; Wang, X.; Chen, C.; Crystal growth and optical properties of  
318 YAl<sub>3</sub>(BO<sub>3</sub>)<sub>4</sub> for UV applications. *J. Cryst. Growth.* **2012**, *341*, 61-65 doi.org/10.1016/j.jcrysGro.2011.12.063

319 30. Dekker, P.; Dawes, J.M.; Characterisation of nonlinear conversion and crystal quality in Nd and Yb doped  
320 YAB. *Opt Expr.* **2004**, *12*, 5922-5930 doi.org/10.1364/OPEX.12.005922

321 31. Dekker, P.; Dawes, J.M. Twinning and natural quasi-phase matching in Yb:YAB. *Appl. Phys. B* **2006**, *83*, 267  
322 doi.org/10.1007/s00340-006-2168-3

323 32. Lutz, F.; Leiss, M.; Muller, J.; Epitaxy of NdAl<sub>3</sub>(BO<sub>3</sub>)<sub>4</sub> for thin film miniature lasers. *J. Cryst. Growth.* **1979**,  
324 47, 130-132 doi.org/10.1016/0022-0248(79)90169-6

325 33. Volkova, E.; Leonyuk, N.; Growth of Yb:YAl<sub>3</sub>(BO<sub>3</sub>)<sub>4</sub> thin films by liquid-phase epitaxy. *J. Cryst. Growth.* **2005**,  
326 275 e2467- e2470. doi.org/10.1016/j.jcrysGro.2004.11.378

327 34. Volkova, E.; Markin, V.; Leonyuk, N.I.; High temperature growth and characterization of  
328 (Er,Yb):YAl<sub>3</sub>(BO<sub>3</sub>)<sub>4</sub> single crystal layers. *J. Cryst. Growth.* **2017**, *468*, 258-261.  
329 doi.or/10.1016/j.jcrysGro.2016.12.036

330 35. Volkova, E.; Maltsev, V.; Kolganova, O.; Leonyuk, N.I.; High temperature growth and characterization of  
331 Er,Yb:YAl<sub>3</sub>(BO<sub>3</sub>)<sub>4</sub> and NdAl<sub>3</sub>(BO<sub>3</sub>)<sub>4</sub> epitaxial layers. *J. Cryst. Growth.* **2014**, *401*, 547-549  
332 doi.org/10.1016/j.jcrysGro.2014.01.035

333 36. Tolstik, N.; Heinrich, S.; Kahn, A.; Volkova, E.; Maltsev, V.; Kuleshov, V.; Huber, G.; Leonyuk, N.I.; High  
334 temperature growth and spectroscopic characterization of Er,Yb:YAl<sub>3</sub>(BO<sub>3</sub>)<sub>4</sub> epitaxial thin layers. *Opt Mat.*  
335 **2010**, *32*, 1377-1379. doi:10.1016/j.optmat.2010.03.016

336 37. Mills, A.D.; Crystallographic data for new rare earth borate compounds RX<sub>3</sub>(BO<sub>3</sub>)<sub>4</sub> *Inorg. Chem.* **1962**, *1* 960-  
337 961 doi:10.1021/ic50004a063